



1 **Rapid mass growth and enhanced light extinction of atmospheric aerosols during the heating**  
2 **season haze episodes in Beijing revealed by aerosol-chemistry-radiation-boundary layer**  
3 **interaction**

4

5 Zhuohui Lin<sup>1</sup>, Yonghong Wang<sup>2</sup>, Feixue Zheng<sup>1</sup>, Ying Zhou<sup>1</sup>, Yishuo Guo<sup>1</sup>, Zemin Feng<sup>1</sup>, Chang Li<sup>1</sup>,  
6 Yusheng Zhang<sup>1</sup>, Simo Hakala<sup>2</sup>, Tommy Chan<sup>2</sup>, Chao Yan<sup>2</sup>, Kaspar R. Daellenbach<sup>2</sup>, Biwu Chu<sup>3</sup>,  
7 Lubna Dada<sup>2</sup>, Juha Kangasluoma<sup>1,2</sup>, Lei Yao<sup>2</sup>, Xiaolong Fan<sup>1</sup>, Wei Du<sup>2</sup>, Jing Cai<sup>2</sup>, Runlong Cai<sup>2</sup>, Tom  
8 V. Kokkonen<sup>2,4</sup>, Putian Zhou<sup>2</sup>, Lili Wang<sup>5</sup>, Tuukka Petäjä<sup>2,4</sup>, Federico Bianchi<sup>1,2</sup>, Veli-Matti  
9 Kerminen<sup>2,4</sup>, Yongchun Liu<sup>1</sup>, and Markku Kulmala<sup>1,2,4</sup>

10

11 <sup>1</sup>Aerosol and Haze Laboratory, Beijing Advanced Innovation Center for Soft Matter Science and  
12 Engineering, Beijing University of Chemical Technology, Beijing, China

13 <sup>2</sup>Institute for Atmospheric and Earth System Research / Physics, Faculty of Science, University of  
14 Helsinki, Finland

15 <sup>3</sup>Research Center for Eco-Environmental Sciences, Chinese Academy of Science, Beijing, China

16 <sup>4</sup>Joint international research Laboratory of Atmospheric and Earth System sciences (JirLATEST),  
17 Nanjing University, Nanjing, China

18 <sup>5</sup>State Key Laboratory of Atmospheric Boundary Layer Physics and Atmospheric Chemistry (LAPC),  
19 Institute of Atmospheric Physics, Chinese Academy of Sciences, Beijing 100029, China

20

21

22

23 Corresponding author: Yonghong Wang

24 E-mail: yonghong.wang@helsinki.fi

25 Submitted to: Atmospheric Chemistry and Physics

26



27 **Abstract**

28

29 Despite the numerous studies investigating haze formation mechanism in China, it is still puzzling  
30 that intensive haze episodes could form within hours directly following relatively clean periods. Haze  
31 has been suggested to be initiated by the variation of meteorological parameters and then to be  
32 substantially enhanced by aerosol-radiation-boundary layer feedback. However, knowledge on the  
33 detailed chemical processes and the driving factors for extensive aerosol mass accumulation during  
34 the feedback is still scarce. Here, the dependency of the aerosol number size distribution, mass  
35 concentration and chemical composition on the daytime mixing layer height (MLH) in urban Beijing  
36 is investigated. The size distribution and chemical composition-resolved dry aerosol light extinction  
37 is also explored. The results indicate that the aerosol mass concentration and fraction of nitrate  
38 increased dramatically when the MLH decreased from high to low conditions, corresponding to  
39 relatively clean and polluted conditions, respectively. Particles having their dry diameters in the size  
40 of ~400-700 nm, and especially particle-phase ammonium nitrate and liquid water, contributed  
41 greatly to visibility degradation during the winter haze periods. The dependency of aerosol  
42 composition on the MLH revealed that ammonium nitrate and aerosol water content increased the  
43 most during low MLH conditions, which may have further triggered enhanced formation of sulphate  
44 and organic aerosol via heterogeneous reactions. As a result, more sulphate, nitrate and water soluble  
45 organics were formed, leading to an enhanced water uptake ability and increased light extinction by  
46 the aerosols. The results of this study contribute towards a more detailed understanding of the aerosol-  
47 chemistry-radiation-boundary layer feedback that is likely to be responsible for explosive aerosol  
48 mass growth events in urban Beijing.

49

50

51

52

53

54



55 **1. Introduction**

56 Despite the recent reduction of air pollutants and their precursors in China between 2013 and 2017,  
57 the current emission and air pollution levels are still substantially high (Wang et al., 2020b; Zheng et  
58 al., 2018). Such high emissions, combined with specific meteorological conditions, frequently lead  
59 to severe haze episodes (An et al., 2019; Wang et al., 2019). Particulate matter, a major air pollutant,  
60 has considerable effects on climate, human health and visibility degradation (Che et al., 2007;  
61 Lelieveld et al., 2015; Spracklen et al., 2008; Wang et al., 2015).

62

63 During winter haze episodes, a rapid growth of the aerosol mass concentration has commonly been  
64 observed, and this phenomenon seems to be directly affected by meteorological factors (Li et al.,  
65 2018b; Liu et al., 2018, 2019b; Wang et al., 2018a, 2014a). The meteorological conditions and  
66 increased aerosol concentrations are proposed to be interlinked by a feedback loop, called the aerosol-  
67 chemistry-boundary layer feedback, in which aerosol particles reduce both solar radiation reaching  
68 the surface and turbulent kinetic energy of the near-surface air (Ding et al., 2016; Petäjä et al., 2016;  
69 Wang et al., 2020d). The increased stability of the boundary layer leads to enhanced air pollution in  
70 the mixed layer, which further suppresses the development of boundary layer. As a consequence,  
71 concentrations of primary aerosol particles, water vapor and relative humidity increase, creating more  
72 favourable conditions for homogeneous and heterogeneous on aerosol surfaces or inside them (Cheng  
73 et al., 2016a; Wang et al., 2016; Wu et al., 2018). Such reactions cause rapid formation of secondary  
74 aerosol matter and enhanced light extinction during severe winter haze episodes. However, more  
75 detailed information on the aerosol and reactive gas chemistry during the aerosol-chemistry-boundary  
76 layer feedback and related rapid aerosol mass growth events is still needed (Liu et al., 2019). For  
77 instance, it is still unclear which chemical reactions and which compounds in the particulate matter  
78 play key roles during such rapid mass growth events.

79

80 The particle number size distribution and chemical composition are considered to be the most  
81 important variables influencing the light extinction by aerosol particles. In the atmosphere, the highest  
82 contribution to aerosol light extinction comes from organic compounds, nitrate and sulphate in



83 particles with diameters of a few hundred nm. This is due to the dominant mass fractions of the  
84 aforementioned compounds in aerosols that correspond to the peak intensity of solar radiation at  
85 wavelengths around 550 nm (Jimenez et al., 2009; Swietlicki et al., 2008). In addition, light scattering  
86 which contributes the most to the light extinction by atmospheric aerosols, can be substantially  
87 enhanced by the presence of liquid water in the aerosol (Chen et al., 2014; Liu et al., 2019a; Pan et  
88 al., 2009; Wang et al., 2020). Hence, quantifying the response of light extinction to different chemical  
89 compounds would be helpful in evaluating the feedbacks associated with secondary aerosol  
90 production.

91

92 In this study, we focus on the physical and chemical properties of aerosols in Beijing during the winter  
93 heating season from October 2018 to February 2019 using state-of-the-art instrumentation. The  
94 variation of aerosol chemical composition and the associated light extinction coefficient as a function  
95 of the varying mixing layer height are discussed. Our aim is to identify the key chemical components  
96 which contribute to the aerosol-chemistry-radiation-boundary layer feedback loop in Beijing.

97

## 98 **2. Methodology**

### 99 **2.1. Measurement location and instrumentations**

100 Measurements were conducted between 1 October 2018 and 28 February 2019 at the roof top of the  
101 university building at the west campus of Beijing University of Chemical Technology (39.95°N,  
102 116.31°E). This station is located about 150 m away from the nearest road (Zizhuyuan road) and 500  
103 m away from the West Third Ring Road, and it is surrounded by commercial properties and residential  
104 dwellings representative of an urban environment. More details on the location can be found in (Liu  
105 et al., 2020; Zhou et al., 2020).

106

107 The meteorological data for this work include basic meteorological variables (relative humidity (RH),  
108 temperature, wind speed, wind direction, and visibility) and mixing layer height (MLH) measured



109 using a weather station (Vaisala Inc., Finland) and a Ceilometer CL51 (Vaisala Inc., Finland),  
110 respectively. The MLH is defined as the height above the surface, through which relatively vigorous  
111 vertical mixing occurs (Holzworth, 1972), and its value is highly related to the vertical temperature  
112 structure and, to some extent, to a mechanically-induced turbulence (Baxter, 1991). Here, we  
113 followed the method introduced earlier by Munkel et al. (2007) and Eresmaa et al. (2012) in  
114 determining the MLH.

115

116 The number concentration of clusters or small aerosol particles in the size range from 1.3-2.5 nm and  
117 the number size distributions of aerosol particles from 6 nm to 840 nm were measured by a Particle  
118 Sizer Magnifier (PSM) and a Differential Mobility Particle Sizer (DMPS), respectively (Aalto et al.,  
119 2001; Vanhanen et al., 2011). The mass concentration of fine particulate matter (PM<sub>2.5</sub>) was measured  
120 using a Tapered Element Oscillating Microbalance Dichotomous Ambient Particulate Monitor  
121 (TEOM 1405-DF, Thermo Fisher Scientific Inc, USA) with a total flow rate of 16.67 L/min (Wang  
122 et al., 2014).

123

124 A time-of-flight aerosol chemical speciation monitor (ToF-ACSM, Aerodyne Research Inc.) was used  
125 to measure the concentrations of non-refractory (NR) components, including sulfate, nitrate,  
126 ammonium, chloride and organics of PM<sub>2.5</sub> (Fröhlich et al., 2013). The inlet flow was set at 1.4 cm<sup>3</sup>/s.  
127 The particle beam passed through the chamber and reached the heated porous tungsten surface  
128 (T≈600°C). There, the non-refractory PM<sub>2.5</sub> constituents were vaporized and then ionized by electrons  
129 (E<sub>kin</sub>=70eV, emitted by a tungsten filament). The ions were measured by a detector and the data was  
130 analyzed using Tofware ver. 2.5.13 within IgorPro ver. 6.3.7.2 (WaveMetrics). The relative ionization  
131 efficiencies (RIE) for sulfate, nitrate, ammonium, chloride and organics applied were 0.86, 1.05, 4.0,  
132 1.5 and 1.4, respectively. In addition to the RIE corrections, CO<sub>2</sub><sup>+</sup>/NO<sub>3</sub> artifact correction and  
133 collection efficiency (CE) correction (Pieber et al., 2016) were also applied to the data. Mass  
134 concentrations of ammonium nitrate, ammonium sulfate and ammonium chloride were determined  
135 according to the method introduced by Gysel et al. (2007). The aerosol liquid water content (AWC)  
136 was calculated by thermodynamic equilibrium model ISORROPIA II using ToF-ACSM data



137 (Fountoukis and Nenes, 2007).

138

139 Highly-oxygenated organic molecules (HOMs) were measured by a chemical ionization long time-  
140 of-flight mass spectrometer equipped with a nitrate chemical ionization source (LToF-CIMS,  
141 Aerodyne Research, Inc. USA) (Jokinen et al., 2012) similar to gas-phase sulfuric acid. Organic  
142 carbon (OC) and element carbon (EC) concentrations were measured semi-continuously with a 1-  
143 hour time resolution using an OC/EC Analyzer (Model-4, Sunset Lab. Inc.).

144

145 The air mass history was studied by calculating particle retroplumes using a Lagrangian particle  
146 dispersion model FLEXPART (FLEXible PARTicle dispersion model) ver. 9.02 (Stohl et al., 2005).  
147 The ECMWF (European Centre for Medium-Range Weather Forecast) operational forecast (with 0.15°  
148 horizontal and 1 h temporal resolution) was used as the meteorological input into the model. During  
149 the measurement period, a new release of 50 000 test particles, distributed evenly between 0 and 100  
150 m above the measurement site, occurred every 1 hour. The released particles were traced backwards  
151 in time for 72 h, unless they exceeded the model boundary (20–60°N, 95–135°E).

152

## 153 **2.2. Aerosol light extinction calculation**

154 The aerosol light extinction coefficient was calculated with the Mie-Model, which uses particle  
155 number size distribution, mass concentrations of different aerosol compounds and their refractive  
156 index as inputs (Seinfeld and Pandis, 2006). We introduced a series of assumptions into the Mie-  
157 Model, including 1) “internal mixture” which considers each chemical component in a particle as  
158 homogeneously mixed with each other; 2) all particles are spherical; and 3) particles of different sizes  
159 have the same chemical composition.

160

161 The practical method introduced under those assumptions in previous studies were found to be  
162 capable of estimating a variation trend of optical property of PM<sub>0.5–20</sub> with a relatively good accuracy  
163 (Lin et al., 2013).



164

165 Table 1. Summary of the parameters for calculating the average optical refractive index.

166

Specie	$\rho_i(\text{g cm}^{-3})$	$n_i$	$k_i$
(NH <sub>4</sub> ) <sub>2</sub> SO <sub>4</sub>	1.760	1.530	0.000
NH <sub>4</sub> NO <sub>3</sub>	1.725	1.554	0.000
NH <sub>4</sub> Cl	1.527	1.639	0.000
Organics	1.400	1.550	0.001
EC	1.500	1.800	0.540

167

168 The average optical refractive index (AORI) of an internally-mixed particle can be calculated from  
169 the optical refractive indices (ORI) of each chemical component by following a mixing rule of  
170 volume-averaged chemical components as  $AORI = n_{\text{eff}} + k_{\text{eff}} \times i$ , where the real part ( $n_{\text{eff}}$ ) and  
171 imaginary part ( $k_{\text{eff}}$ ) are given by:

$$n_{\text{eff}} = \left( \sum_i n_i \cdot m_i / \rho_i \right) / \left( \sum_i m_i / \rho_i \right) \quad (1)$$

$$k_{\text{eff}} = \left( \sum_i k_i \cdot m_i / \rho_i \right) / \left( \sum_i m_i / \rho_i \right) \quad (2)$$

172 Here  $m_i$  and  $\rho_i$  are the mass concentration and density of the component  $i$  in particles, respectively,  
173 and  $n_i$  and  $k_i$  are the real and imaginary parts of ORI of this component, respectively. The  
174 parameters for calculating the AORI are summarised in Table 1. The values of  $n_i$  and  $k_i$  in Table 1  
175 are referenced to the light wavelength of 550 nm.

176

177  $Q_{sp,j}$  represents light scattering efficiency of a single particle with diameter  $D_j$ , while  $Q_{ep,j}$   
178 represents light absorption efficiency. Theoretically,  $Q_{sp,j}$  and  $Q_{ep,j}$  are both the function of  $D_j$  and  
179 the  $AORI_j$  (the AORI of the particle with diameter  $D_j$ ) at a given light wavelength  $\lambda$ , for which the  
180 complicated calculations were referenced to a previous publication. Regarding the limitations of  
181 measurement techniques, the  $AORI_j$  was assumed to be equal to the  $AORI_{\text{PM}_{2.5}}$ , which was



182 determined based on chemical composition of PM<sub>2.5</sub>. It is possible to derive expressions for the cross  
183 sections of a spherical particle exactly. The formulas for  $Q_{sp,j}$  and  $Q_{ep,j}$  are:

184

$$Q_{sp,j}(D_j, \lambda, AORI_j) = \frac{2}{\alpha^2} \sum_{k=1}^{\infty} (2k+1) \cdot [|a_k|^2 + |b_k|^2] \quad (3)$$

$$Q_{ep,j}(D_j, \lambda, AORI_j) = \frac{2}{\alpha^2} \sum_{k=1}^{\infty} (2k+1) \cdot \text{Re}[a_k + b_k] \quad (4)$$

185

186 where

187

$$a_k = \frac{\alpha \psi'_k(y) \psi_k(\alpha) - y \psi'_k(\alpha) \psi_k(y)}{\alpha \psi'_k(y) \xi_k(\alpha) - y \xi'_k(\alpha) \psi_k(y)}$$

189

$$b_k = \frac{y \psi'_k(y) \psi_k(\alpha) - \alpha \psi'_k(\alpha) \psi_k(y)}{y \psi'_k(y) \xi_k(\alpha) - \alpha \xi'_k(\alpha) \psi_k(y)}$$

191

192 with  $y = \alpha m$ .

193

$$m = n_{eff} + i \cdot k_{eff}$$

195

$$\alpha = \frac{\pi D_j}{\lambda}$$

197

198 with  $\lambda = 550$  nm.

199

200 where complex number  $m$  stands for  $AORI_j$ , while  $\alpha$  is the size of the particle, usually expressed as

201 a dimensionless size parameter. The functions  $\psi_k(z)$  and  $\xi_k(z)$  are the Riccati–Bessel functions:

$$\psi_k(z) = \left(\frac{\pi z}{2}\right)^{1/2} J_{k+1/2}(z) \quad (5)$$

$$\xi_k(z) = \left(\frac{\pi z}{2}\right)^{1/2} [J_{k+1/2}(z) + i(-1)^k J_{-k-1/2}(z)] \quad (6)$$

202



203 where  $J_{k+1/2}$  and  $J_{-k-1/2}$  are the Bessel functions of the first kind and their footnotes indicate the  
204 order of Bessel functions. The Mie theory can serve as the basis of a computational procedure to  
205 calculate the scattering and absorption of light by any sphere as a function of wavelength.

206

207 According to the Mie-Model,  $b_{sp}$  (light scattering coefficient) and  $b_{ep}$  (light extinction coefficient)  
208 can be quantified with Eqs. (5) and (6), respectively.  $b_{ap}$  (light absorption coefficient) is the  
209 difference between  $b_{ep}$  and  $b_{sp}$ , which equals zero, when  $k_i$  equals zero or very small. Optical  
210 properties including  $b_{ep}$ ,  $b_{sp}$  and  $b_{ap}$  to be discussed later are all referenced to light wavelength of  
211 550 nm.

$$b_{sp} = \sum_j b_{sp,j} = \sum_j \frac{\pi D_j^2}{4} \cdot Q_{sp,j}(D_j, \lambda, AORI_j) \cdot N_j \quad (7)$$

$$b_{ep} = \sum_j b_{ep,j} = \sum_j \frac{\pi D_j^2}{4} \cdot Q_{ep,j}(D_j, \lambda, AORI_j) \cdot N_j \quad (8)$$

212

213

214 In Eqs. (7) and (8),  $D_j$  stands for the median Stokes diameter in the  $j$ -th particle size range and  $N_j$  is  
215 the number concentration of particles with diameter,  $D_j$ .

216

### 217 3. Results and discussion

#### 218 3.1. Typical case of rapid aerosol mass growth episodes affected by aerosol-chemistry- 219 boundary layer interactions

220 An example of rapid aerosol mass growth in urban wintertime Beijing is illustrated in Figure 1, where  
221 the haze accumulation was associated with a rapid  $PM_{2.5}$  mass concentration increase from few  $\mu\text{g}/\text{m}^3$   
222 to more than  $100 \mu\text{g}/\text{m}^3$  in less than 7 hours. A haze episode started on afternoon 20 February 2019  
223 under stagnant meteorological conditions with low wind speeds and elevated ambient relative  
224 humidity (Figure S1). The polluted periods during this case occurred under southerly wind transport



225 conditions, whereas clean air masses originated from the north-westerly regions (as shown in Figure  
226 S2, S3). These are typical features for a haze evolution process in Beijing (Wang et al., 2020b). During  
227 the haze periods marked by the shaded areas in Figure 1, an obvious increase of chemical mass  
228 concentration was observed by the ToF-ACSM, characterised by high concentrations of secondary  
229 aerosol components (nitrate, organics and sulphate) and typically a shallow boundary layer. The mass  
230 concentrations of organics, sulphate and nitrate increased dramatically with a decreasing MLH,  
231 accounting for 88.5% of NR-PM<sub>2.5</sub> during the rapid aerosol mass growth period. The aerosol mass  
232 growth was the fastest for nitrate. The mass concentrations of organic and elemental carbon followed  
233 that of NR-PM<sub>2.5</sub>.

234

235 The MLH reached its maximum at around 14:00 in the afternoon of 20 February, after which the  
236 development of the mixing layer was suppressed and MLH decreased with the arrival of pollution  
237 (Figure 1a). Previous studies have shown that the aerosol-radiation-boundary layer feedback  
238 contributes to a rapid enhancement of air pollution (Petäjä et al., 2016; Wang et al., 2020d). High  
239 concentrations of aerosol particles obscure downward radiation, as a result of which the surface  
240 temperature and sensitive heat flux decrease and the development of mixing layer height is suppressed.  
241 Recent studies have gradually realized that the facilitation of various chemical processes play a non-  
242 negligible role in the aerosol-radiation-boundary layer feedback (Liu.Q et al., 2018; Liu.Z et al., 2019).  
243 Therefore, it is important to identify and quantify the role of different specific chemical species and  
244 particle size ranges in reducing atmospheric radiation and extinction.

245

246 Figure 2 shows the contributions of size and chemical composition-resolved dry aerosol to light  
247 extinction during the investigated period. As the pollution intensified and MLH decreased (Fig 1c),  
248 the light extinction of atmospheric aerosols increased significantly. Assuming that particles of  
249 different sizes have the same chemical composition as PM<sub>2.5</sub> (organics, NH<sub>4</sub>NO<sub>3</sub>, EC, (NH<sub>4</sub>)<sub>2</sub>SO<sub>4</sub>,  
250 NH<sub>4</sub>Cl), the light extinction of particles in the size range of 300-700 nm increased significantly from  
251 the relative clean period to the polluted period (namely from 12:00 to 16:00). During relatively clean  
252 conditions, the contributions of organics, NH<sub>4</sub>NO<sub>3</sub>, EC, (NH<sub>4</sub>)<sub>2</sub>SO<sub>4</sub> and NH<sub>4</sub>Cl to the total aerosol



253 light extinction were 42%, 23%, 18%, 11% and 7%, respectively. The contribution of  $\text{NH}_4\text{NO}_3$  to  
254 aerosol light extinction reached 40% during the heavily polluted period. The increased light extinction  
255 by aerosols reduced solar radiation reaching the surface, so that the development of the boundary  
256 layer was suppressed.

257

### 258 **3.2. Connection between the aerosol chemical composition, light extinction, size distribution** 259 **and MLH during the heating season**

260

261 To better characterize the effect of the chemical composition of dry aerosols and the PNSD (particle  
262 number size distribution) light extinction under different MLH conditions, the daytime (8:00 – 16:00  
263 LT) measurement data from October 2018 to February 2019 were selected for further analysis. As  
264 shown by Figure 3 and consistent with other observations in Beijing (Tang et al., 2016; Wang et al.,  
265 2020c), there was a general tendency for the  $\text{PM}_{2.5}$  mass concentration to increase with a decreasing  
266 MLH. Organic compounds and nitrate were the most abundant fractions of the daytime aerosol mass  
267 composition, contributing together approximately 70% to total NR- $\text{PM}_{2.5}$  mass concentration. With a  
268 decreasing MLH, the fraction of nitrate mass in NR- $\text{PM}_{2.5}$  slightly increased while that of organics  
269 decreased. This feature makes the aerosol more hygroscopic under low MLH conditions typical for  
270 heavily polluted periods. The increased nitrate fraction in the aerosol could also enhance the  
271 formation of other secondary aerosol components (Xue et al., 2019). Note that some fraction of  
272 aerosol nitrate could consist of organic nitrate originating from reaction of peroxy radical with nitric  
273 oxide; however, it is difficult to distinguish organic nitrate from inorganic nitrate at the moment due  
274 to instrumental limitations (Fröhlich et al., 2013).

275

276 Figure 4 depicts the calculated daytime light extinction of the dry aerosol as a function of the MLH,  
277 separated by different size ranges and chemical components. We may see that in general, particles  
278 with dry diameters in the range of 300-700 nm explained more than 80% of the total aerosol light  
279 extinction (Figure 4b). Similar to their share in NR- $\text{PM}_{2.5}$ , the fraction of light extinction by



280 ammonium nitrate increased and that of organics decreased during the lowest MLH conditions  
281 corresponding to the heavy pollution periods (Figure 4d). There are also apparent differences in the  
282 relative contribution of different particle size ranges to light extinction in different MLH conditions:  
283 with a decreasing MLH, the contribution of particles with dry dimeters larger than about 400-500 nm  
284 clearly increased while that of sub-300 nm particles notably decreased. This indicates that the  
285 enhanced light extinction by the dry aerosol at low MLH conditions was not only due the more  
286 abundant aerosol mass concentration, but also due to the growth of individual particles to optically  
287 more active sizes.

288

289 At relative humidity larger than about 70%, aerosol liquid water gives a significant contribution to  
290 the aerosol mass concentration and often a dominant contribution to the aerosol light extinction (Titos  
291 et al., 2016). This has important implications for the aerosol-chemistry-radiation-boundary layer  
292 feedback, when considering our findings listed above and further noting that heavy pollution periods  
293 are often accompanied by high values of RH in Beijing (Zhong et al., 2018). First, compared to clean  
294 or moderately-polluted conditions, the enhancement in the aerosol light extinction under polluted is  
295 probably much larger than that illustrated in Figure 4. Second, the high aerosol water content under  
296 polluted conditions promotes many kinds of chemical reactions taking place on the surface or inside  
297 aerosol particles.

298

### 299 **3.3. Aerosol-chemistry-radiation-boundary layer interaction**

300

301 In order to further investigate the interaction between MLH and chemical compounds (either observed  
302 or calculated), we divided the observed  $PM_{2.5}$  concentrations into highly polluted and less polluted  
303 conditions using a threshold value of  $75 \mu g m^{-3}$  for  $PM_{2.5}$ . The organics, nitrate, ammonium, sulfate,  
304 chloride, HOM, aerosol water content (AWC) and  $PM_{2.5}$  as a function of the mixing layer height  
305 during both highly polluted and less polluted conditions are shown in Figure 5. The fitted relationships  
306 connecting the concentrations of different chemical compounds to the reduction of MLH under highly



307 and less polluted conditions allowed us to estimate the net mass concentration increase of each  
308 compound due to secondary formation and aerosol-chemical-boundary layer feedback under highly  
309 polluted conditions (shaded areas in Figure 5). It is worth noting that AWC, nitrate and sulfate  
310 increased the most as the MLH decreased, as represented by the large shaded areas in Figs. 5 (h), (b)  
311 and (c). The day-time nitrate in aerosol is formed predominately via the reaction of nitric acid and  
312 ammonium, while nitric acid is produced from gas phase reaction of nitrogen dioxide and hydroxy  
313 radical (Seinfeld and Pandis, 2006). High concentrations of daytime nitrate aerosols indicate efficient  
314 production of gas phase nitric acid, its partitioning into liquid aerosol and its fast neutralization by  
315 abundant ammonia (Li et al., 2018a; Pan et al., 2016; Wang et al., 2020). A recent study shows that  
316 condensation of nitric acid and ammonia could promote fast growth of newly formed particle in urban  
317 environment condition (Wang et al., 2020d). Another possibility is that ammonium nitrate is formed  
318 rapidly on particle surfaces due to the hydrolysis of dinitrogen pentoxide ( $N_2O_5$ ) during daytime, as  
319 the AWC increased significantly (Wang et al., 2014; Wang et al., 2020). However, a quantitative  
320 distinction between the two formation pathways for nitrate formation is not possible in this study. The  
321 dramatic increase of nitrate aerosol could also promote the formation of sulfate by heterogeneous  
322 reactions (Cheng et al., 2016b; Wang et al., 2016). The concentration of HOMs showed a slight  
323 increase as the MLH decreased, which suggests that also the formation of HOMs is enhanced with an  
324 increased level of air pollution. This phenomenon should be further investigated as HOMs can  
325 substantially contribute to the secondary organic aerosol formation.

326

327 Figure 6 displays the dry aerosol light extinction by different chemical compounds in the same way  
328 as Fig. 5 did for aerosol mass concentrations. The aerosol light extinction is directly related to the  
329 reduction of solar radiation reaching the surface, assuming that aerosol chemical components are  
330 vertically nearly homogeneously distributed. The light extinction from ammonium nitrate,  
331 ammonium sulfate and organics showed significantly increased contributions under highly polluted  
332 conditions (low MLH) as compared with less polluted conditions. To the contrary, no such  
333 enhancement was observed for ammonium chloride or element carbon (Figs. 6 (d) and (e)). In case  
334 of EC this is an expected result, as it originates solely from primary sources. The formation of particle



335 phase chloride have secondary sources from chlorine atom-initiated oxidation of volatile organic  
336 compounds, so that the resulting oxidation products could contribute to the observed chloride (Wang  
337 and Ruiz, 2017; Wang et al., 2019a).

338

339 To better illustrate the combined effects of secondary aerosol formation and associated feedback on  
340 the daytime mass concentrations and light extinction due to different chemical components, we scaled  
341 these quantities by either the total  $PM_{2.5}$  mass concentration or EC concentration and plotted them as  
342 a function of MLH (Fig. 7). The latter scaling minimizes the boundary layer accumulation effect on  
343 our analysis, as EC originates from primary emission sources (Cao et al., 2006). As shown in Fig. 7a,  
344 organics with their mass fraction of 61% were the most abundant component in  $PM_{2.5}$  under high  
345 MLH conditions, followed by nitrate and ammonium with their mass fractions of 22% and 13%,  
346 respectively. The aerosol was estimated to be rather dry under high MLH conditions ( $AWC/PM_{2.5} =$   
347 0.03). However, with the decreasing MLH, the fraction of nitrate and the  $AWC$  to  $PM_{2.5}$  ratio increased  
348 up to 45% and 0.2, respectively. This clearly indicates rapid nitrate formation and dramatic increase  
349 of the aerosol water uptake from less polluted conditions to intensive haze pollution. Compared with  
350 EC (Fig. 7c), the concentrations of organic compounds, nitrate, sulfate and ammonium increased by  
351 factors of 1.5, 6.3, 4.8 and 4.9 respectively, from the highest to the lowest MLH conditions. Thus,  
352 although organics remained as the second most abundant aerosol component after nitrate under haze  
353 conditions, secondary formation and associated feedback from less to highly polluted conditions were  
354 clearly stronger for both sulfate and ammonium. Efficient sulfate production associated with haze  
355 formation has been reported in several studies conducted in China (Cheng et al., 2016; Xie et al.,  
356 2015; Xue et al., 2016). Ammonium production during haze formation is tied with neutralization of  
357 acidic aerosol by ammonia, which was apparently present abundantly in the gas phase. Compared  
358 with the EC concentration, light extinction by  $(NH_4NO_3)$  increased the most from the highest MLH  
359 conditions ( $248 M m^{-1}/\mu g m^{-3}$ ) to the lowest MLH conditions ( $1150 M m^{-1}/\mu g m^{-3}$ ) as shown by Figure  
360 7b. Overall, the rapid growth of nitrate aerosol mass, together with abundant concentration of organic  
361 aerosol, were the main cause of the light extinction for dry aerosol under haze formation.

362



363 The mechanism governing the aerosol-chemistry-radiation-boundary layer feedback for the rapid  
364 growth of atmospheric aerosol is illustrated in Fig. 8. As a result of reduction in solar radiation and  
365 atmospheric heating, a variety of chemical reactions in the gas phase and on particle surfaces or inside  
366 them are enhanced with an increased relative humidity and AWC. Such conditions are unfavorable  
367 for the dispersion of pollutants, which further enhances atmospheric stability. The formation of  
368 hydrophilic compounds, e.g., nitrate, sulfate and oxygenated organic compounds, result in enhanced  
369 water uptake by aerosol particles, which will essentially increase heterogeneous reactions associated  
370 with these particles. As a result, the aerosol mass and size increase, light extinction is enhanced, and  
371 the development of the mixing layer is depressed. At the same time, aerosol precursors concentrated  
372 within a shallower mixing layer lead to enhanced production rate of aerosol components in both gas  
373 and aerosol phases, especially nitrate but also other secondary aerosol. The increased concentrations  
374 of aerosol will further enhance this positive loop.

375

#### 376 **4. Conclusions**

377

378 We investigated the synergetic variations of aerosol chemical composition and mixing layer height  
379 during the daytime in urban Beijing. Significant dependency of the sharp increase of ammonium  
380 nitrate and aerosol water content with the occurrence of the explosive aerosol mass growth events  
381 were observed. We showed that these two components drove a positive aerosol-chemistry-radiation-  
382 boundary layer feedback loop, which played an important role in the explosive aerosol mass growth  
383 events. A plausible explanation is that the increased aerosol water content at low mixing layer heights  
384 provides favorable conditions for heterogeneous reactions for nitrate and sulfate production and  
385 neutralization by ammonia. The significant formation of secondary aerosol increases the  
386 concentration of aerosol particles in the diameter range 300-700 nm, which effectively reduces the  
387 solar radiation reaching the surface and further enhances the aerosol-chemistry-radiation-boundary  
388 layer feedback loop. Our analysis connects the aerosol light extinction to a reduction in the mixing  
389 layer height, which suppresses the volume into which air pollutants are emitted and leads to an



390 explosive aerosol mass growth. Our results indicate that reduction of ammonium and nitrate  
391 concentration in aerosol could weaken the aerosol-radiation-chemistry-boundary layer feedback loop,  
392 which could thereby reduce heavy haze episodes in Beijing.

### 393 **5. Acknowledgements**

394 This work was supported by the funding from Beijing University of Chemical Technology. The  
395 European Research Council via advanced grant ATM-GTP (project no. 742206) and Academy of  
396 Finland via Academy professor project of M. K.

### 397 **6. Competing financial interests**

398 The authors declare no competing financial interests.

### **7. Author contributions**

399 YW and MK initiated the study. ZL, YW, FZ, YZ, YG, ZF, CL, YZ, TC, CY, KD, BC, JK, LY, XF,  
400 WD, JC and YL conducted the longtime measurements. ZL, YW, LD, RC, SH, PZ, LW, VK, YL and  
401 MK interpreted the data. ZL, YW and VK wrote the manuscript.

402

403

404

405



## 406 Reference

- Aalto, P., Hämeri, K., Becker, E. D. O., Weber, R., Salm, J., Mäkelä, J. M., Hoell, C., O'Dowd, C. D., Karlsson, H., Hansson, H., Väkevä, M., Koponen, I. K., Buzorius, G. and Kulmala, M.: Physical characterization of aerosol particles during nucleation events, *Tellus, Series B: Chemical and Physical Meteorology*, 53(4), 344–358, doi:10.3402/tellusb.v53i4.17127, 2001.
- An, Z., Huang, R.-J., Zhang, R., Tie, X., Li, G., Cao, J., Zhou, W., Shi, Z., Han, Y., Gu, Z. and Ji, Y.: Severe haze in northern China: A synergy of anthropogenic emissions and atmospheric processes, *Proceedings of the National Academy of Sciences*, 116(18), 8657 LP – 8666, doi:10.1073/pnas.1900125116, 2019.
- Baxter, R.: Determination of mixing heights from data collected during the 1985 SCCAMP field program, *Journal of Applied Meteorology*, 30(5), 598–606, doi:10.1175/1520-0450(1991)030<0598:DOMHFD>2.0.CO;2, 1991.
- Cao, G., Zhang, X. and Zheng, F.: Inventory of black carbon and organic carbon emissions from China, *Atmospheric Environment*, 40(34), 6516–6527, doi:10.1016/j.atmosenv.2006.05.070, 2006.
- Che, H., Zhang, X., Li, Y., Zhou, Z. and Qu, J. J.: Horizontal visibility trends in China 1981–2005, *Geophysical Research Letters*, 34(24), doi:10.1029/2007GL031450, 2007.
- Chen, J., Zhao, C. S., Ma, N. and Yan, P.: Aerosol hygroscopicity parameter derived from the light scattering enhancement factor measurements in the North China Plain, *Atmos. Chem. Phys.*, 14, 8105–8118, doi:10.5194/acp-14-8105-2014, 2014.
- Cheng, Y., Zheng, G., Wei, C., Mu, Q., Zheng, B., Wang, Z., Gao, M., Zhang, Q., He, K., Carmichael, G., Pöschl, U. and Su, H.: Reactive nitrogen chemistry in aerosol water as a source of sulfate during haze events in China, *Science Advances*, 2(12), e1601530–e1601530, doi:10.1126/sciadv.1601530, 2016b.
- Ding, A. J., Huang, X., Nie, W., Sun, J. N., Kerminen, V. M., Petäjä, T., Su, H., Cheng, Y. F., Yang, X. Q., Wang, M. H., Chi, X. G., Wang, J. P., Virkkula, A., Guo, W. D., Yuan, J., Wang, S. Y., Zhang, R. J., Wu, Y. F., Song, Y., Zhu, T., Zilitinkevich, S., Kulmala, M. and Fu, C. B.: Enhanced haze pollution by black carbon in megacities in China, *Geophysical Research Letters*, 43(6), 2873–2879, doi:10.1002/2016GL067745, 2016.



Eresmaa, N., Härkönen, J., Joffre, S. M., Schultz, D. M., Karppinen, A. and Kukkonen, J.: A Three-Step Method for Estimating the Mixing Height Using Ceilometer Data from the Helsinki Testbed, *Journal of Applied Meteorology and Climatology*, 51(12), 2172–2187, doi:10.1175/JAMC-D-12-058.1, 2012.

Fountoukis, C. and Nenes, A.: ISORROPIA II: a computationally efficient thermodynamic equilibrium model for

$\text{K}^+$ – $\text{Ca}^{2+}$ – $\text{Mg}^{2+}$ – $\text{NH}_4^+$ – $\text{Na}^+$ – $\text{SO}_4^{2-}$ – $\text{NO}_3$ , *Atmospheric Chemistry and Physics*, 7(17), 4639–4659, doi:10.5194/acp-7-4639-2007, 2007.

Fröhlich, R., Cubison, M. J., Slowik, J. G., Bukowiecki, N., Prévôt, A. S. H., Baltensperger, U., Schneider, J., Kimmel, J. R., Gonin, M., Rohner, U., Worsnop, D. R. and Jayne, J. T.: The ToF-ACSM: A portable aerosol chemical speciation monitor with TOFMS detection, *Atmospheric Measurement Techniques*, 6(11), 3225–3241, doi:10.5194/amt-6-3225-2013, 2013.

Gysel, M., Crosier, J., Topping, D. O., Whitehead, J. D., Bower, K. N., Cubison, M. J., Williams, P. I., Flynn, M. J., McFiggans, G. B. and Coe, H.: Closure study between chemical composition and hygroscopic growth of aerosol particles during TORCH2, *Atmospheric Chemistry and Physics*, 7(24), 6131–6144, doi:10.5194/acp-7-6131-2007, 2007.

Holzworth, G. C.: Mixing heights, wind speeds, and potential for urban air pollution throughout the contiguous united states, , 118, 1972.

Jimenez, J. L., Canagaratna, M. R., Donahue, N. M., Prevot, A. S. H., Zhang, Q., Kroll, J. H., DeCarlo, P. F., Allan, J. D., Coe, H., Ng, N. L., Aiken, A. C., Docherty, K. S., Ulbrich, I. M., Grieshop, A. P., Robinson, A. L., Duplissy, J., Smith, J. D., Wilson, K. R., Lanz, V. A., Hueglin, C., Sun, Y. L., Tian, J., Laaksonen, A., Raatikainen, T., Rautiainen, J., Vaattovaara, P., Ehn, M., Kulmala, M., Tomlinson, J. M., Collins, D. R., Cubison, M. J., Dunlea, E. J., Huffman, J. A., Onasch, T. B., Alfarra, M. R., Williams, P. I., Bower, K., Kondo, Y., Schneider, J., Drewnick, F., Borrmann, S., Weimer, S., Demerjian, K., Salcedo, D., Cottrell, L., Griffin, R., Takami, A., Miyoshi, T., Hatakeyama, S., Shimono, A., Sun, J. Y., Zhang, Y. M., Dzepina, K., Kimmel, J. R., Sueper, D., Jayne, J. T., Herndon, S. C., Trimborn, A. M., Williams, L. R., Wood, E. C., Middlebrook, A. M., Kolb, C. E., Baltensperger, U. and Worsnop, D. R.: Evolution of organic



- aerosols in the atmosphere, *Science*, 326(5959), 1525–1529, doi:10.1126/science.1180353, 2009.
- Jokinen, T., Sipilä, M., Junninen, H., Ehn, M., Lönn, G., Hakala, J., Petäjä, T., Mauldin, R. L., Kulmala, M. and Worsnop, D. R.: Atmospheric sulphuric acid and neutral cluster measurements using CI-API-TOF, *Atmospheric Chemistry and Physics*, 12(9), 4117–4125, doi:10.5194/acp-12-4117-2012, 2012.
- Lelieveld, J., Evans, J. S., Fnais, M., Giannadaki, D. and Pozzer, A.: The contribution of outdoor air pollution sources to premature mortality on a global scale, *Nature*, 525(7569), 367–371, doi:10.1038/nature15371, 2015.
- Li, H., Zhang, Q., Zheng, B., Chen, C., Wu, N., Guo, H., Zhang, Y., Zheng, Y., Li, X. and He, K.: Nitrate-driven urban haze pollution during summertime over the North China Plain, *Atmospheric Chemistry and Physics*, 18(8), 5293–5306, doi:10.5194/acp-18-5293-2018, 2018a.
- Li, J., Sun, J., Zhou, M., Cheng, Z., Li, Q., Cao, X. and Zhang, J.: Observational analyses of dramatic developments of a severe air pollution event in the Beijing area, *Atmospheric Chemistry and Physics*, 18(6), 3919–3935, doi:10.5194/acp-18-3919-2018, 2018b.
- Lin, Z. J., Tao, J., Chai, F. H., Fan, S. J., Yue, J. H., Zhu, L. H., Ho, K. F. and Zhang, R. J.: Impact of relative humidity and particles number size distribution on aerosol light extinction in the urban area of Guangzhou, *Atmospheric Chemistry and Physics*, 13(3), 1115–1128, doi:10.5194/acp-13-1115-2013, 2013.
- Liu, G., Xin, J., Wang, X., Si, R., Ma, Y., Wen, T., Zhao, L., Zhao, D., Wang, Y. and Gao, W.: Impact of the coal banning zone on visibility in the Beijing-Tianjin-Hebei region, *Science of the Total Environment*, 692, 402–410, doi:10.1016/j.scitotenv.2019.07.006, 2019a.
- Liu, Q., Jia, X., Quan, J., Li, J., Li, X., Wu, Y., Chen, D., Wang, Z. and Liu, Y.: New positive feedback mechanism between boundary layer meteorology and secondary aerosol formation during severe haze events, *Scientific Reports*, 8(1), doi:10.1038/s41598-018-24366-3, 2018.
- Liu, Y., Zhang, Y., Lian, C., Yan, C. and Feng, Z.: The promotion effect of nitrous acid on aerosol formation in wintertime Beijing : possible contribution of traffic-related emission, *Atmos. Chem. Phys. Discuss.*, 2020(February), 1–43, doi:10.5194/acp-2020-150, 2020.
- Liu, Z., Hu, B., Ji, D., Cheng, M., Gao, W., Shi, S., Xie, Y., Yang, S., Gao, M., Fu, H., Chen, J. and



- Wang, Y.: Characteristics of fine particle explosive growth events in Beijing, China: Seasonal variation, chemical evolution pattern and formation mechanism, *Science of the Total Environment*, 687, 1073–1086, doi:10.1016/j.scitotenv.2019.06.068, 2019b.
- Münel, C., Eresmaa, N., Räsänen, J. and Karppinen, A.: Retrieval of mixing height and dust concentration with lidar ceilometer, *Boundary-Layer Meteorology*, 124(1), 117–128, doi:10.1007/s10546-006-9103-3, 2007.
- Pan, X. L., Yan, P., Tang, J., Ma, J. Z., Wang, Z. F., Gbaguidi, A. and Sun, Y. L.: Observational study of influence of aerosol hygroscopic growth on scattering coefficient over rural area near Beijing mega-city, *Atmospheric Chemistry and Physics*, 9(19), 7519–7530, doi:10.5194/acp-9-7519-2009, 2009.
- Pan, Y., Tian, S., Liu, D., Fang, Y., Zhu, X., Zhang, Q., Zheng, B., Michalski, G. and Wang, Y.: Fossil Fuel Combustion-Related Emissions Dominate Atmospheric Ammonia Sources during Severe Haze Episodes: Evidence from 15N-Stable Isotope in Size-Resolved Aerosol Ammonium, *Environmental Science and Technology*, 50(15), 8049–8056, doi:10.1021/acs.est.6b00634, 2016.
- Petäjä, T., Järvi, L., Kerminen, V. M., Ding, A. J., Sun, J. N., Nie, W., Kujansuu, J., Virkkula, A., Yang, X., Fu, C. B., Zilitinkevich, S. and Kulmala, M.: Enhanced air pollution via aerosol-boundary layer feedback in China, *Scientific Reports*, 6, doi:10.1038/srep18998, 2016.
- Pieber, S. M., El Haddad, I., Slowik, J. G., Canagaratna, M. R., Jayne, J. T., Platt, S. M., Bozzetti, C., Daellenbach, K. R., Fröhlich, R., Vlachou, A., Klein, F., Dommen, J., Miljevic, B., Jiménez, J. L., Worsnop, D. R., Baltensperger, U. and Prévôt, A. S. H.: Inorganic Salt Interference on CO<sub>2</sub><sup>+</sup> in Aerodyne AMS and ACSM Organic Aerosol Composition Studies, *Environmental Science and Technology*, 50(19), 10494–10503, doi:10.1021/acs.est.6b01035, 2016.
- Spracklen, D. V., Carslaw, K. S., Kulmala, M., Kerminen, V. M., Sihto, S. L., Riipinen, I., Merikanto, J., Mann, G. W., Chipperfield, M. P., Wiedensohler, A., Birmili, W. and Lihavainen, H.: Contribution of particle formation to global cloud condensation nuclei concentrations, *Geophysical Research Letters*, 35(6), doi:10.1029/2007GL033038, 2008.
- Stohl, A., Forster, C., Frank, A., Seibert, P. and Wotawa, G.: Technical note: The Lagrangian particle dispersion model FLEXPART version 6.2, *Atmospheric Chemistry and Physics*, 5(9),



2461–2474, doi:10.5194/acp-5-2461-2005, 2005.

Swietlicki, E., Hansson, H.-C., Hämeri, K., Svenningsson, B., Massling, A., Mcfiggans, G., Mcmurry, P. H., Petäjä, T., Tunved, P., Gysel, M., Topping, D., Weingartner, E., Baltensperger, U., Rissler, J., Wiedensohler, A. and Kulmala, M.: Hygroscopic properties of submicrometer atmospheric aerosol particles measured with H-TDMA instruments in various environments—a review, *Tellus B: Chemical and Physical Meteorology*, 60(3), 432–469, doi:10.1111/j.1600-0889.2008.00350.x, 2008.

Tang, G., Zhang, J., Zhu, X., Song, T., Munkel, C., Hu, B., Schäfer, K., Liu, Z., Zhang, J., Wang, L., Xin, J., Suppan, P. and Wang, Y.: Mixing layer height and its implications for air pollution over Beijing, China, *Atmos. Chem. Phys.*, 16, 2459–2475, doi:10.5194/acp-16-2459-2016, 2016.

Titos, G., Cazorla, A., Zieger, P., Andrews, E., Lyamani, H., Granados-Muñoz, M. J., Olmo, F. J. and Alados-Arboledas, L.: Effect of hygroscopic growth on the aerosol light-scattering coefficient: A review of measurements, techniques and error sources, *Atmospheric Environment*, 141, 494–507, doi:10.1016/j.atmosenv.2016.07.021, 2016.

Vanhanen, J., Mikkilä, J., Lehtipalo, K., Sipilä, M., Manninen, H. E., Siivola, E., Petäjä, T. and Kulmala, M.: Particle size magnifier for nano-CN detection, *Aerosol Science and Technology*, 45(4), 533–542, doi:10.1080/02786826.2010.547889, 2011.

Wang, G., Zhang, R., Gomez, M. E., Yang, L., Zamora, M. L., Hu, M., Lin, Y., Peng, J., Guo, S., Meng, J., Li, J., Cheng, C., Hu, T., Ren, Y., Wang, Y., Gao, J., Cao, J., An, Z., Zhou, W., Li, G., Wang, J., Tian, P., Marrero-Ortiz, W., Secret, J., Du, Z., Zheng, J., Shang, D., Zeng, L., Shao, M., Wang, W., Huang, Y., Wang, Y., Zhu, Y., Li, Y., Hu, J., Pan, B., Cai, L., Cheng, Y., Ji, Y., Zhang, F., Rosenfeld, D., Liss, P. S., Duce, R. A., Kolb, C. E. and Molina, M. J.: Persistent sulfate formation from London Fog to Chinese haze, *Proceedings of the National Academy of Sciences of the United States of America*, 113(48), 13630–13635, doi:10.1073/pnas.1616540113, 2016.

Wang, H., Peng, Y., Zhang, X., Liu, H., Zhang, M., Che, H. and Cheng, Y.: Contributions to the explosive growth of PM<sub>2.5</sub> mass due to aerosol – radiation feedback and decrease in turbulent diffusion during a red alert heavy haze in Beijing – Tianjin – Hebei, China, , 17717–17733, 2018a.

Wang, J., Wang, S., Jiang, J., Ding, A., Zheng, M., Zhao, B., Wong, D. C., Zhou, W., Zheng, G.,



- Wang, L., Pleim, J. E. and Hao, J.: Impact of aerosol-meteorology interactions on fine particle pollution during China's severe haze episode in January 2013, *Environmental Research Letters*, 9(9), doi:10.1088/1748-9326/9/9/094002, 2014a.
- Wang, M., Kong, W., Marten, R., He, X.-C., Chen, D., Pfeifer, J., Heitto, A., Kontkanen, J., Dada, L., Kürten, A., Yli-Juuti, T., Manninen, H. E., Amanatidis, S., Amorim, A., Baalbaki, R., Baccarini, A., Bell, D. M., Bertozzi, B., Bräkling, S., Brilke, S., Murillo, L. C., Chiu, R., Chu, B., De Menezes, L.-P., Duplissy, J., Finkenzeller, H., Carracedo, L. G., Granzin, M., Guida, R., Hansel, A., Hofbauer, V., Krechmer, J., Lehtipalo, K., Lamkaddam, H., Lampimäki, M., Lee, C. P., Makhmutov, V., Marie, G., Mathot, S., Mauldin, R. L., Mentler, B., Müller, T., Onnela, A., Partoll, E., Petäjä, T., Philippov, M., Pospisilova, V., Ranjithkumar, A., Rissanen, M., Rörup, B., Scholz, W., Shen, J., Simon, M., Sipilä, M., Steiner, G., Stolzenburg, D., Tham, Y. J., Tomé, A., Wagner, A. C., Wang, D. S., Wang, Y., Weber, S. K., Winkler, P. M., Wlasits, P. J., Wu, Y., Xiao, M., Ye, Q., Zauner-Wieczorek, M., Zhou, X., Volkamer, R., Riipinen, I., Dommen, J., Curtius, J., Baltensperger, U., Kulmala, M., Worsnop, D. R., Kirkby, J., Seinfeld, J. H., El-Haddad, I., Flagan, R. C. and Donahue, N. M.: Rapid growth of new atmospheric particles by nitric acid and ammonia condensation, *Nature*, 581(7807), 184–189, doi:10.1038/s41586-020-2270-4, 2020d.
- Wang, X., Wang, T., Yan, C., Tham, Y. J., Xue, L., Xu, Z. and Zha, Q.: Large daytime signals of N<sub>2</sub>O<sub>5</sub> and NO<sub>3</sub> inferred at 62 amu in a TD-CIMS: Chemical interference or a real atmospheric phenomenon, *Atmospheric Measurement Techniques*, 7(1), 1–12, doi:10.5194/amt-7-1-2014, 2014b.
- Wang, Y., Riva, M., Xie, H. and Heikkinen, L.: Formation of highly oxygenated organic molecules from chlorine atom initiated oxidation of alpha-pinene, *Atmospheric Chemistry and Physics*, 2020, 1–31, doi:10.5194/acp-2019-807, 2020.
- Wang, Y., Wang, Y., Wang, L., Petäjä, T., Zha, Q., Gong, C., Li, S., Pan, Y., Hu, B., Xin, J. and Kulmala, M.: Increased inorganic aerosol fraction contributes to air pollution and haze in China, *Atmos. Chem. Phys.*, 19, 5881–5888, doi:10.5194/acp-19-5881-2019, 2019b.
- Wang, Y., Gao, W., Wang, S., Song, T., Gong, Z., Ji, D., Wang, L., Liu, Z., Tang, G., Huo, Y., Tian, S., Li, J., Li, M., Yang, Y., Chu, B., Petäjä, T., Kerminen, V.-M., He, H., Hao, J., Kulmala,



- M., Wang, Y. and Zhang, Y.: Contrasting trends of PM<sub>2.5</sub> and surface ozone concentrations in China from 2013 to 2017, *National Science Review*, doi:10.1093/nsr/nwaa032, 2020b.
- Wang, Y., Chen, Y., Wu, Z., Shang, D., Bian, Y., Du, Z. and Schmitt, S. H.: Mutual promotion between aerosol particle liquid water and particulate nitrate enhancement leads to severe nitrate-dominated particulate matter pollution and low visibility, *Atmos. Chem. Phys.*, (September 2020), 2161–2175, 2020c.
- Wang, Y., Yu, M., Wang, Y., Tang, G., Song, T., Zhou, P., Liu, Z., Hu, B., Ji, D., Wang, L., Zhu, X., Yan, C., Ehn, M., Gao, W., Pan, Y., Xin, J., Sun, Y., Kerminen, V.-M., Kulmala, M. and Petäjä, T.: Rapid formation of intense haze episodes via aerosol–boundary layer feedback in Beijing, *Atmos. Chem. Phys.*, 20(1), 45–53, doi:10.5194/acp-20-45-2020, 2020d.
- Wang, Y. H., Hu, B., Ji, D. S., Liu, Z. R., Tang, G. Q., Xin, J. Y., Zhang, H. X., Song, T., Wang, L. L., Gao, W. K., Wang, X. K. and Wang, Y. S.: Ozone weekend effects in the Beijing-Tianjin-Hebei metropolitan area, China, *Atmos. Chem. Phys.*, 14, 2419–2429, doi:10.5194/acp-14-2419-2014, 2014c.
- Wang, Y. H., Liu, Z. R., Zhang, J. K., Hu, B., Ji, D. S., Yu, Y. C. and Wang, Y. S.: Aerosol physicochemical properties and implications for visibility during an intense haze episode during winter in Beijing, *Atmospheric Chemistry and Physics*, 15(6), 3205–3215, doi:10.5194/acp-15-3205-2015, 2015.
- Wu, Z., Wang, Y., Tan, T., Zhu, Y., Li, M., Shang, D., Wang, H., Lu, K., Guo, S., Zeng, L. and Zhang, Y.: Aerosol Liquid Water Driven by Anthropogenic Inorganic Salts: Implying Its Key Role in Haze Formation over the North China Plain, *Environmental Science and Technology Letters*, 5(3), 160–166, doi:10.1021/acs.estlett.8b00021, 2018.
- Xie, Y., Ding, A., Nie, W., Mao, H., Qi, X., Huang, X., Xu, Z., Kerminen, V. M., Petäjä, T., Chi, X., Virkkula, A., Boy, M., Xue, L., Guo, J., Sun, J., Yang, X., Kulmala, M. and Fu, C.: Enhanced sulfate formation by nitrogen dioxide: Implications from in-situ observations at the SORPES station, *Journal of Geophysical Research*, 120(24), 12,679–12,694, doi:10.1002/2015JD023607, 2015.
- Xue, J., Yuan, Z., Griffith, S. M., Yu, X., Lau, A. K. H. and Yu, J. Z.: Sulfate Formation Enhanced



by a Cocktail of High NO<sub>x</sub>, SO<sub>2</sub>, Particulate Matter, and Droplet pH during Haze-Fog Events in Megacities in China: An Observation-Based Modeling Investigation, *Environmental Science and Technology*, 50(14), 7325–7334, doi:10.1021/acs.est.6b00768, 2016.

Xue, J., Yu, X., Yuan, Z., Griffith, S. M., Lau, A. K. H., Seinfeld, J. H. and Yu, J. Z.: Efficient control of atmospheric sulfate production based on three formation regimes, *Nature Geoscience*, 12(12), 1–6, doi:10.1038/s41561-019-0485-5, 2019.

Zheng, B., Tong, D., Li, M., Liu, F., Hong, C., Geng, G., Li, H., Li, X., Peng, L., Qi, J., Yan, L., Zhang, Y., Zhao, H., Zheng, Y., He, K. and Zhang, Q.: Trends in China’s anthropogenic emissions since 2010 as the consequence of clean air actions, *Atmospheric Chemistry and Physics Discussions*, 1–27, doi:10.5194/acp-2018-374, 2018.

Zhong, J., Zhang, X., Dong, Y., Wang, Y., Liu, C., Wang, J., Zhang, Y. and Che, H.: Feedback effects of boundary-layer meteorological factors on cumulative explosive growth of PM<sub>2.5</sub> during winter heavy pollution episodes in Beijing from 2013 to 2016, *Atmospheric Chemistry and Physics*, 18(1), 247–258, doi:10.5194/acp-18-247-2018, 2018.

Zhou, Y., Dada, L., Liu, Y., Fu, Y., Kangasluoma, J., Chan, T., Yan, C., Chu, B., Daellenbach, K. R., Bianchi, F., Kokkonen, T. V., Liu, Y., Kujansuu, J., Kerminen, V.-M., Petäjä, T., Wang, L., Jiang, J. and Kulmala, M.: Variation of size-segregated particle number concentrations in wintertime Beijing, *Atmospheric Chemistry and Physics*, 20(2), 1201–1216, doi:10.5194/acp-20-1201-2020, 2020.

407

408

409

410

411

412

413

414

415



416

417

418

419

420

421

422

423

424

425

426

427

428

429

430

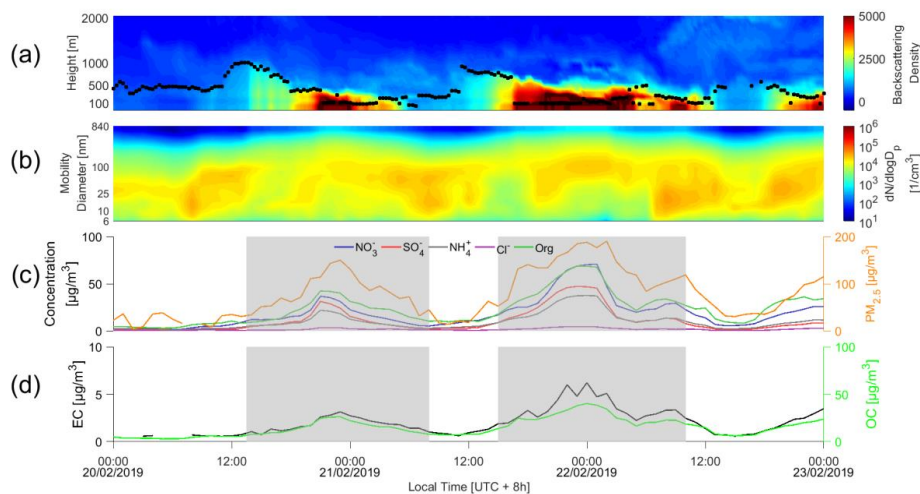
431

432

Figure caption

433

434



435

436

437 Figure 1. Time series of (a) backscattering density and boundary layer height (b) particle number

438 concentration distribution (PNSD), (c) chemical composition species mass concentration and PM<sub>2.5</sub>

439 mass concentrations and (d) elemental carbon (EC) and organic carbon (OC). The haze periods are

440 marked by the shaded areas.

441

442

443

444

445

446

447

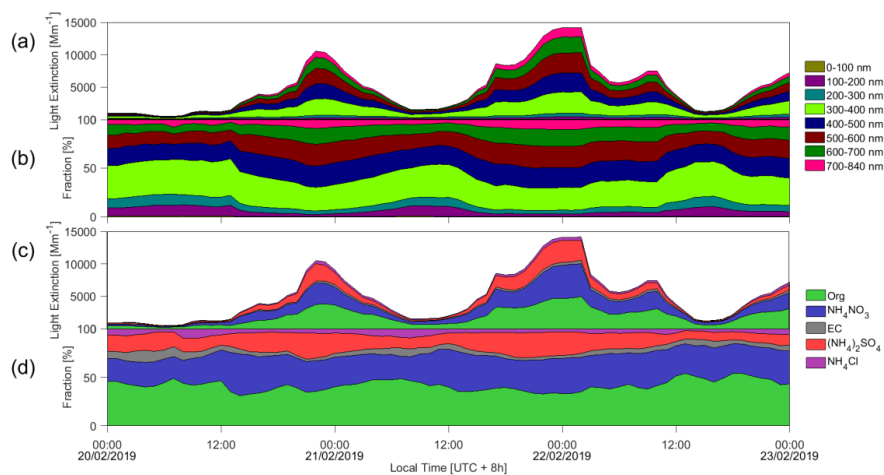
448

449

450

451

452



453

454 Figure 2. Time series of (a, b) variation of light extinction from different size aerosol and fractions,  
455 and (c, d) variation of light extinction from different aerosol species and fractions. The legends in the  
456 left side of figures are particle diameter and chemical compositions, respectively.

457

458

459

460

461

462

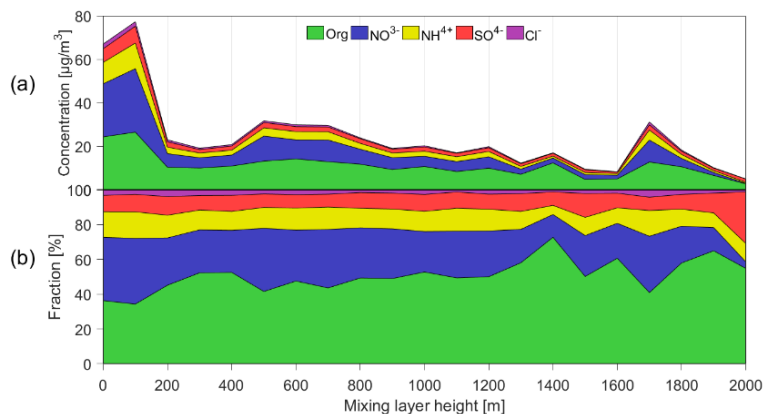
463

464

465

466

467



468

469 Figure 3. Statistical relationship between MLH and concentration (a) and fraction (b) of chemical  
470 composition species. Only daytime conditions determined by ceilometer from non-rainy periods  
471 (RH<95%) are considered.

472

473

474

475

476

477

478

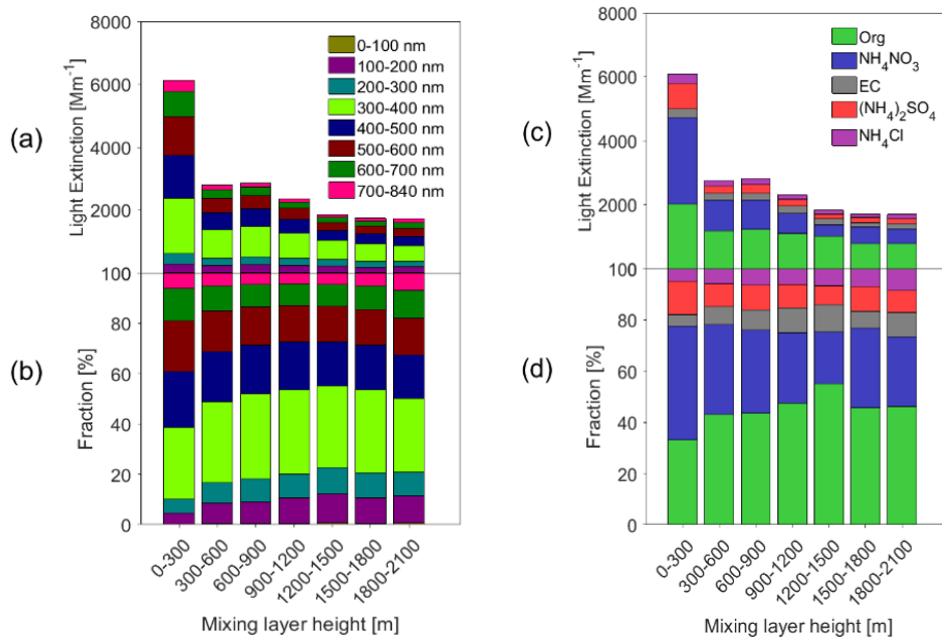
479

480

481

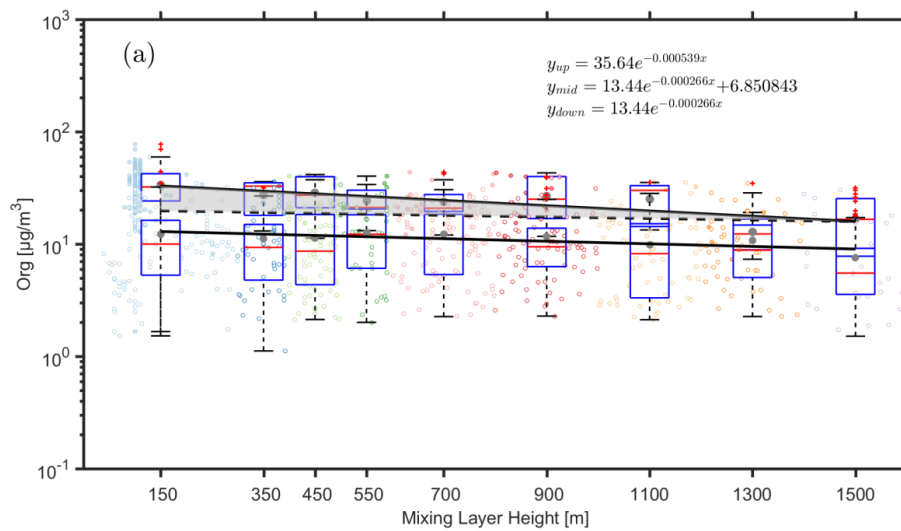
482

483

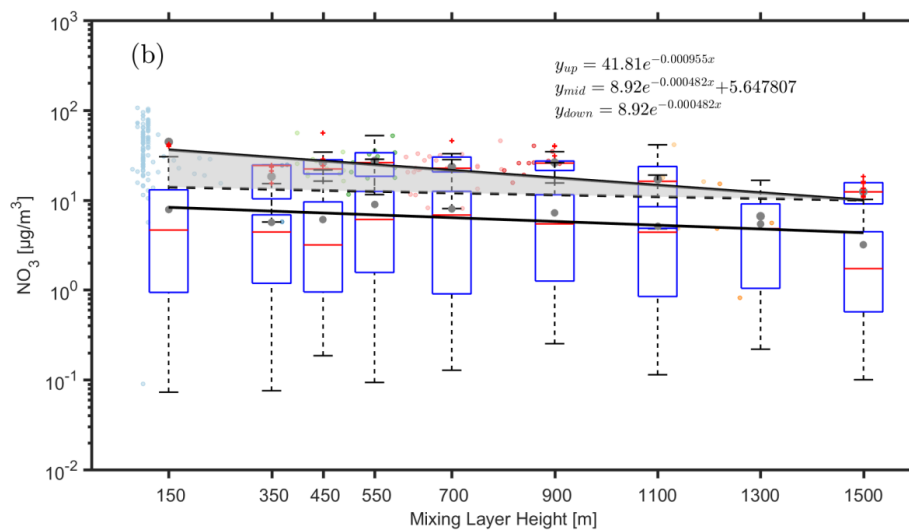


484  
485  
486  
487  
488  
489  
490  
491  
492  
493  
494  
495  
496  
497  
498  
499

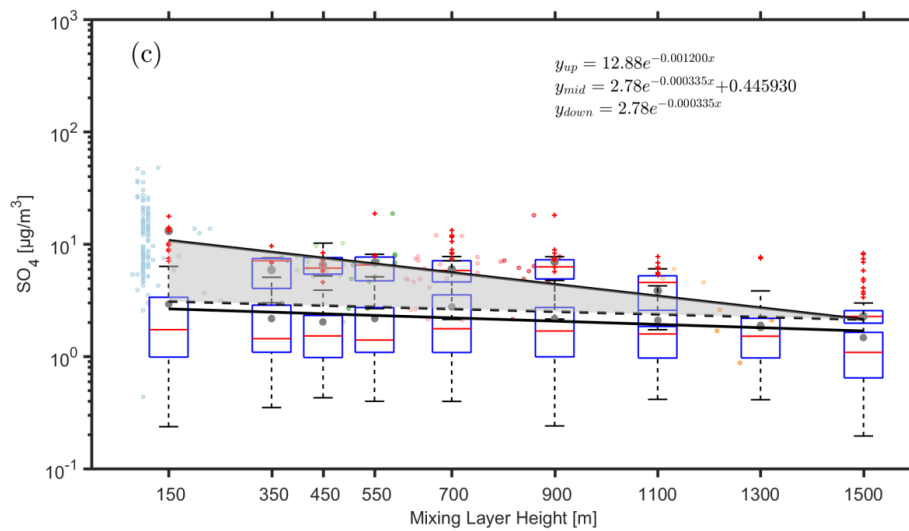
Figure 4. Statistical relationship between MLH and light extinction of different aerosol species. Only daytime conditions determined by the ceilometer from non-rainy periods (RH<95%) are considered.



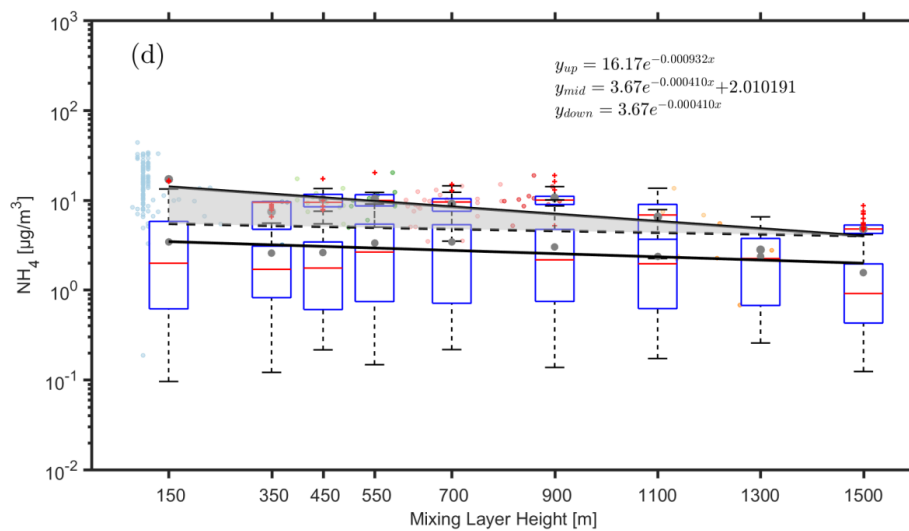
500



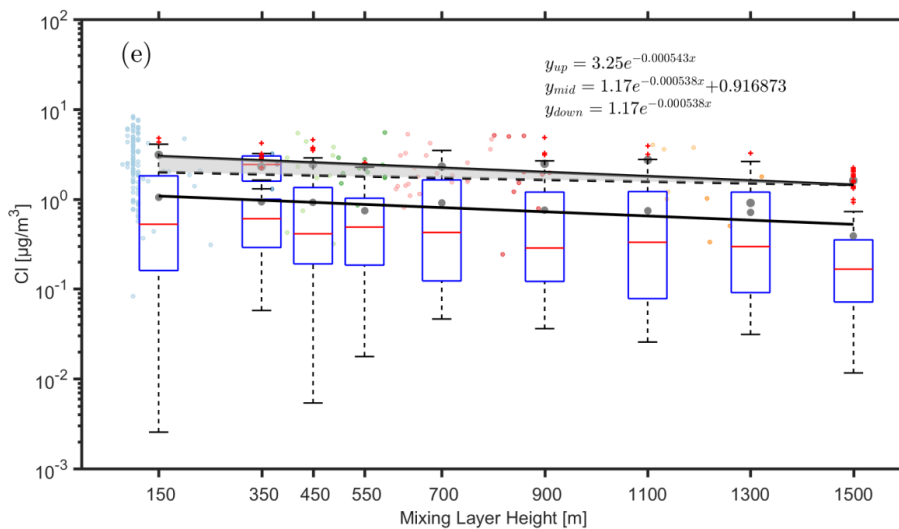
501



502



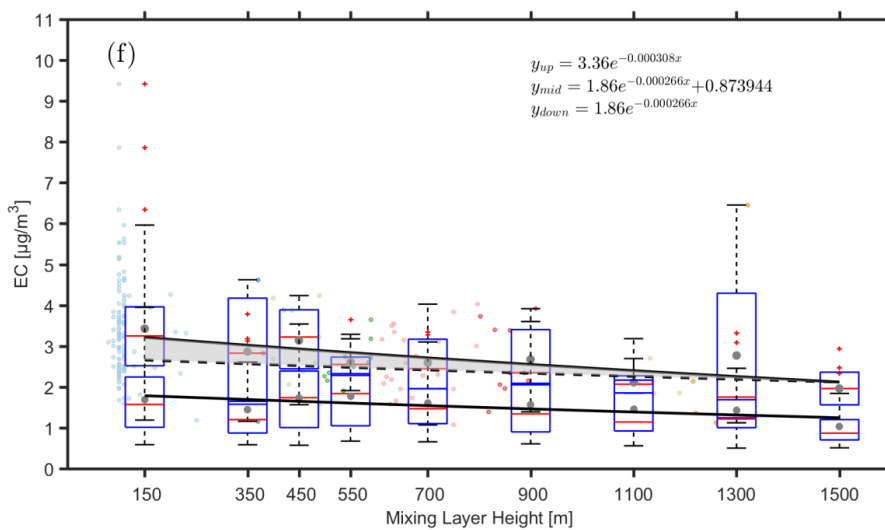
503



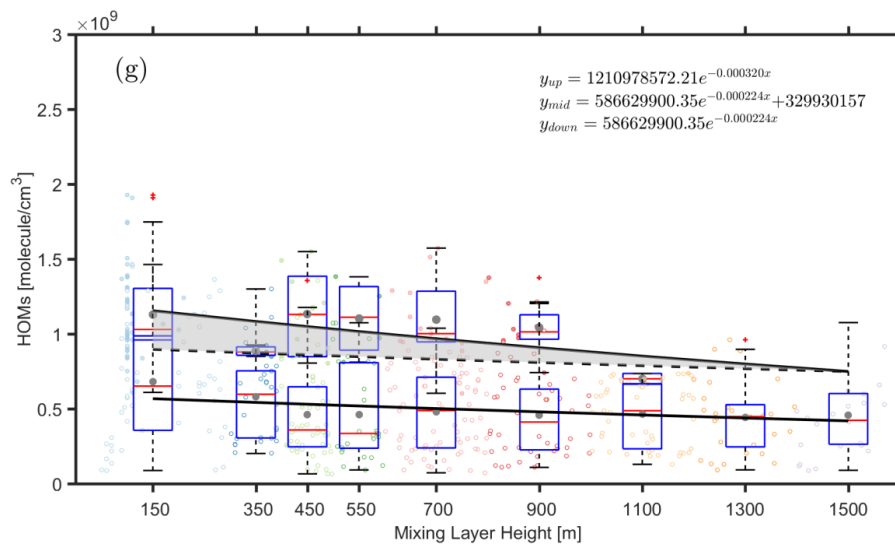
504

505

506

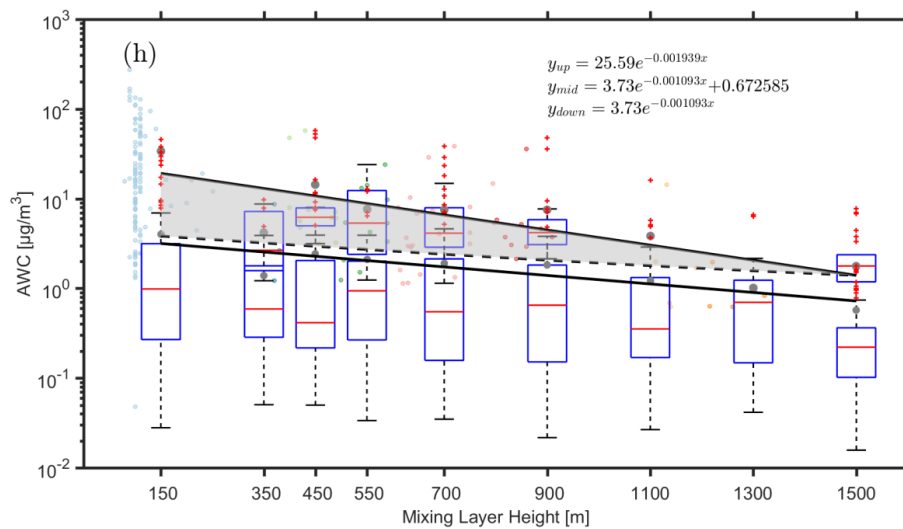


507

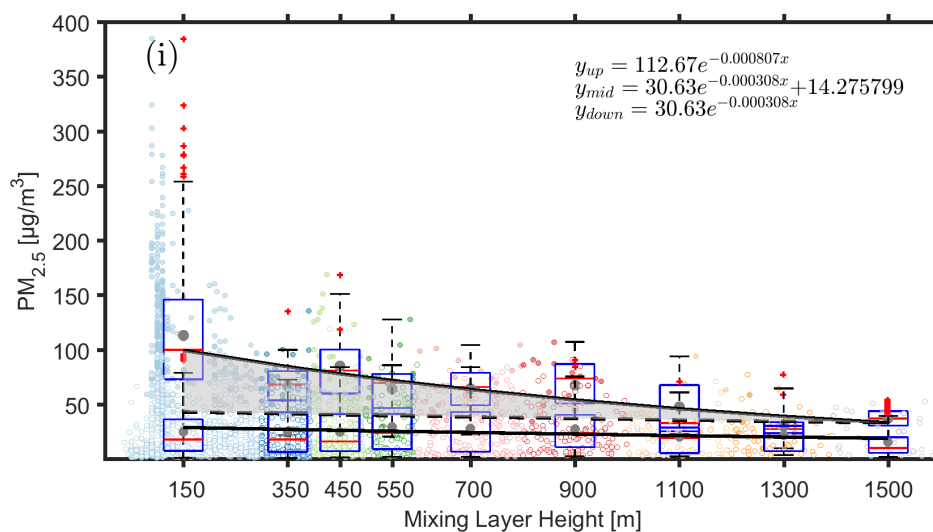


508

509



510



511

512

513 Figure 5. Observed dependency of (organics (a), nitrate (b), ammonium (c), sulfate (d), chlorine (e),  
514 element carbon (f), HOMs (g), AWC (h) and  $PM_{2.5}$ (i) on the MLH during polluted and less-polluted  
515 conditions. The data related to the upper fitting line represents  $PM_{2.5}$  concentrations larger than  $75 \mu g$   
516  $m^{-3}$ , while the data related to the lower fitting line represents  $PM_{2.5}$  concentrations lower than  $75 \mu g$   
517  $m^{-3}$ . Only daytime conditions determined by the ceilometer from non-rainy periods ( $RH < 95\%$ ) were  
518 considered. The dark grey points and red lines in the boxes represent mean and median values,  
519 respectively. The shaded area between the upper solid and dotted lines corresponds to an increased  
520 amount of the specific compounds with decreased MLH, assuming that the compound has the same  
521 variation pattern under highly-polluted conditions as in less-polluted time.

522

523

524

525

526

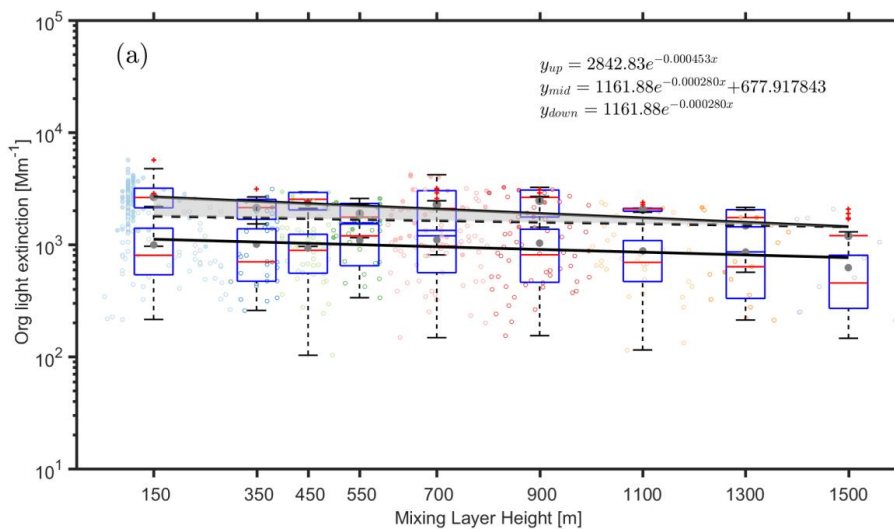
527

528

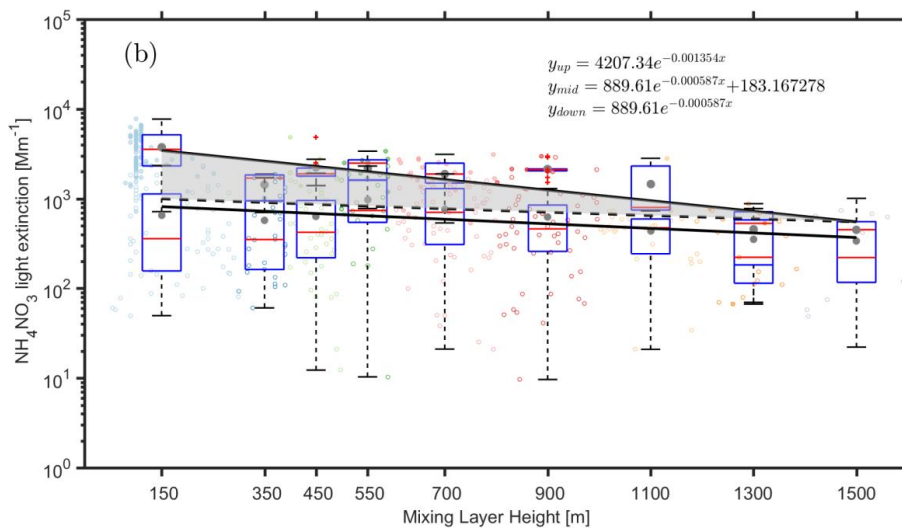
529



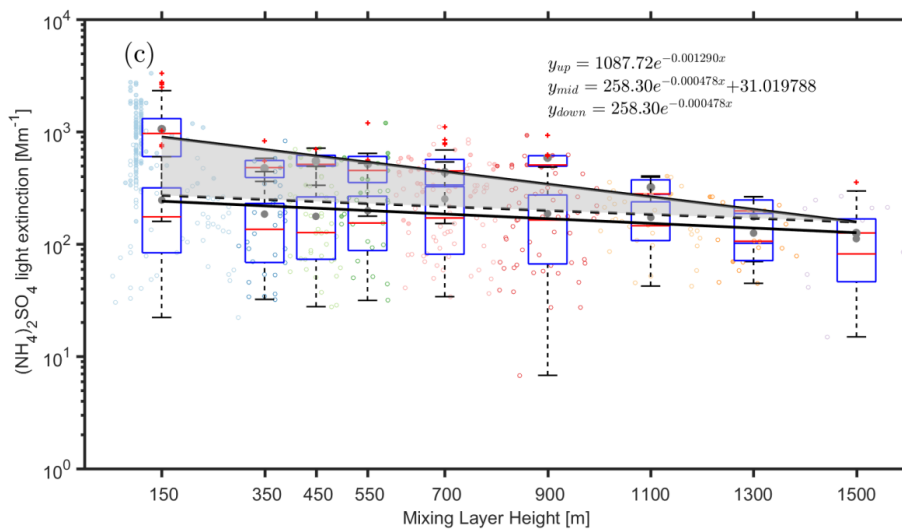
530



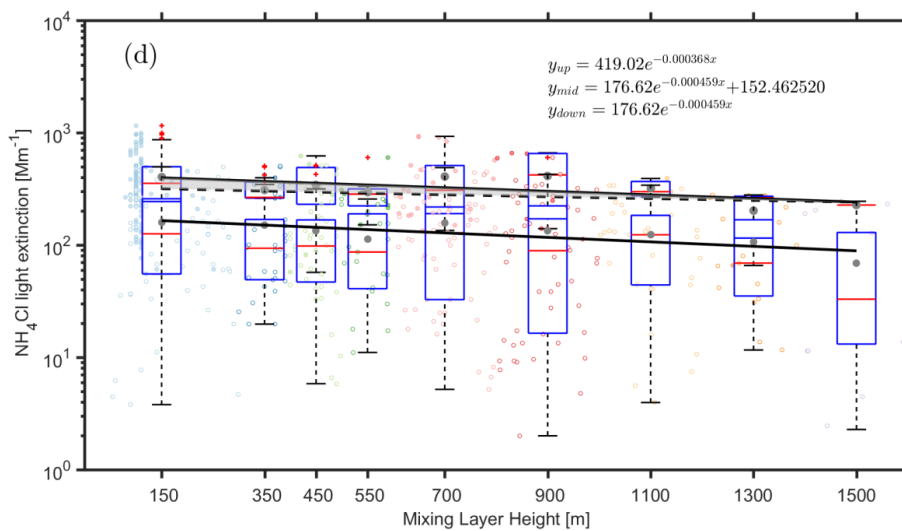
531



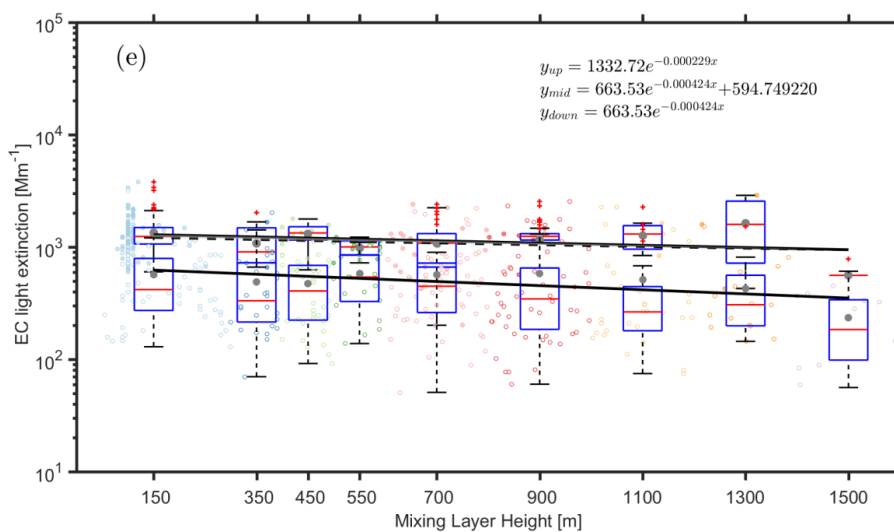
532



533



534



535

536

537

538 Figure 6. Observed dependency of the aerosol light extinction due to  $\text{NH}_4\text{NO}_3$  (a)  $(\text{NH}_4)_2\text{SO}_4$  (b),

539  $\text{NH}_4\text{Cl}$  (c) Org (d) and EC (e) on the MLH during polluted and non-polluted conditions. The data

540 related to the upper fitting line represents  $\text{PM}_{2.5}$  concentrations larger than  $75 \mu\text{g m}^{-3}$ , while the data

541 related to the lower fitting line represents  $\text{PM}_{2.5}$  concentrations less than  $75 \mu\text{g m}^{-3}$ . Only daytime

542 conditions determined by ceilometer from non-rainy periods ( $\text{RH} < 95\%$ ) are considered. The dark

543 grey points and red lines in the boxes represent mean and median values, respectively. The shaded

544 area between the upper solid and dashed line corresponds to an increased amount of  $\text{PM}_{2.5}$  with a

545 decreased MLH, assuming that  $\text{PM}_{2.5}$  has the same variation pattern under highly-polluted conditions

546 as in less polluted time

547

548

549

550

551

552

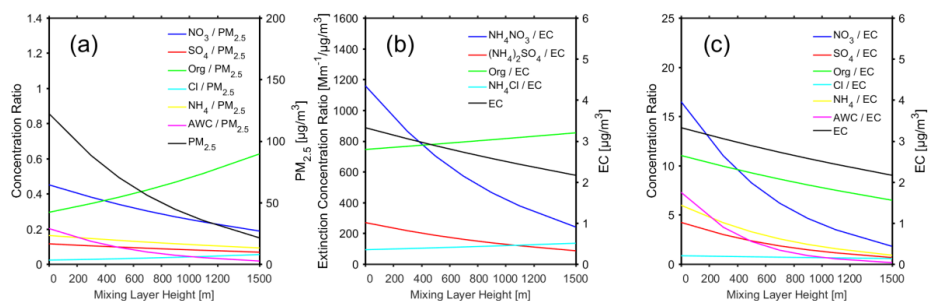
553



554

555

556



557

558 Figure 7. (a) the ratio of the mass concentration of different chemical components (nitrate, sulfate,  
559 organics, chlorine, ammonium) and AWC to the mass concentration of NR\_PM<sub>2.5</sub> as a function of  
560 MLH. (b) the ratio of dry aerosol light extinction by different chemical components (NH<sub>4</sub>NO<sub>3</sub>,  
561 (NH<sub>4</sub>)<sub>2</sub>SO<sub>4</sub>, Org, NH<sub>4</sub>Cl) to the mass concentration EC as a function of MLH (c) the ratio of the mass  
562 concentration of different chemical components (nitrate, sulfate, organics, chlorine, ammonium) and  
563 AWC to the mass concentration of EC as a function of MLH. All the data corresponds to polluted  
564 conditions (fine PM >75 μg m<sup>-3</sup>), and only daytime conditions determined by the ceilometer from  
565 non-rainy periods (RH<95%) were considered.

566

567

568

569

570

571

572

573

574

575

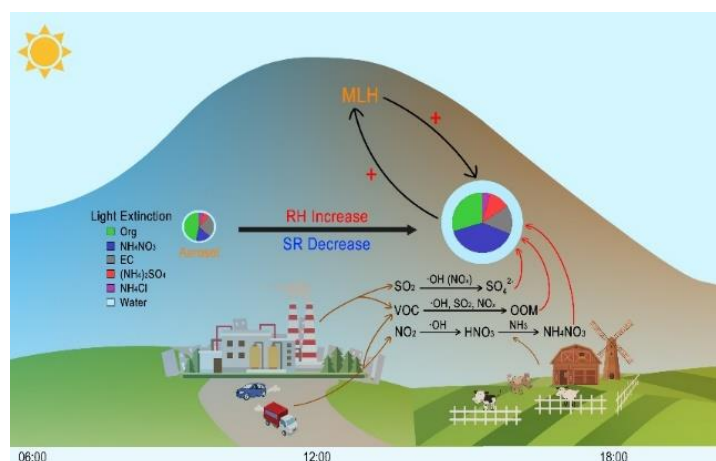


576

577

578

579



580

581 **Figure 8. A schematic picture illustrating the process of rapid aerosol mass growth and enhanced**  
582 **light extinction in Beijing.** The plus symbols represent the strengthening of a specific process. At  
583 the presence of aerosols during afternoon time in Beijing, the intensity of solar radiation reaching the  
584 surface will be decreased and relative humidity will be increased. As a result, the development of  
585 boundary layer will be suppressed, and the concentrations of aerosol precursors (e.g., SO<sub>2</sub>, NO<sub>2</sub>, VOC)  
586 will be increased. In turn, the secondary production of these sulfate, nitrate and oxygenated organic  
587 compounds will be enhanced due to increased concentrations and partitioning of these compounds  
588 into the aerosol phase. The increased formation of secondary aerosol mass will reduce solar radiation  
589 further and the haze formation increased. Noting that during intensive haze periods, nitrate and its  
590 contribution to light extinction contribution increased dramatically.

591

592

593

594

595